

Failure area evaluation of the coupler with threaded bar: Experimental and Numerical study

Mohamad Reza Shokrzadeh¹, F. Nateghi-Alahi², Mohammad Reza Mansoori^{*}, Pasha Javadi¹

Abstract

The problem of overcrowding at the junction of the rebars is very significant, particularly for seismic details. Mechanical couplers can, thus offer an appealing solution that eliminates the disadvantages of traditional reinforcement splicing. By identifying the target area for bar failure, the potential area for failure could be modified. With this in mind, it is very useful in assessing the position of the reinforced concrete (RC) plastic hinge. In this context, the present study focuses on the numerical and analytical modeling of the experimentally obtained responses of integrated bars (without coupler) and bars with mechanical coupler to tensile uniaxial tests. Simulation results showed agreement with the experimental response in terms of the load–elongation curve, Von Mises yield, and failure mode. After validating the model, alternative designs (diameter, height, and thickness of mechanical couplers and bars) were numerically tested to study the influence of the geometry of the structural system on the failure of the mechanical coupler. Overall results indicated that the optimum design would be the one with an increased diameter in the thread area of both the bar and the mechanical coupler. For this improved configuration, the load-bearing capacity was similar to the integrated bar (without coupler) cases.

Keywords: Mechanical bar Splices, Coupler Properties, Ductility, Absorbed energy, Numerical model

Introduction

One of the main concerns of researchers is the significance of bar splice techniques in reinforced concrete (RC) structures in terms of seismic activity and overall construction costs and time. Due to the constraints of bar length, the splicing of bars in RC structures is unavoidable [1,2]. Several methods for splicing reinforcement bars include: overlapping bars, couplers, mechanical

patching, and head-to-head welding. The length of the overlapping bars must be equal to or greater than the length of the anchorage bar when the overlapping procedure is used [3]. For situations in which ductile detailing is needed, reinforcement congestion becomes especially important [4]. Conventional lap splices can lead to section over-reinforcement, leading to a possible non-ductile reaction in the spliced region due to stress localization at both ends of the lap,

✉ m.mansoori@srbiau.ac.ir

1. Department of Civil Engineering, Science and Research Branch, Islamic Azad University, Tehran, Iran

2. International Institute of Earthquake Engineering and Seismology, Tehran, Iran

thus altering the capacity of deformation. The important problem with this approach is that, especially when applied to bars with a diameter greater than 30 mm, it is not economically advantageous. As a result, the use of couplers has become widespread, not only reducing bar weight, minimizing bar congestion, and contributing to cost-effective construction, but also making it easier to apply and less time-consuming [4–6]. There are currently a number of standards available for testing mechanical bar splices [7–9]. However, neither of these documents sets out approval requirements or modeling approaches for couplers to be used in the critical area of ductile members [5]. In recent experimental research, coupler efficiency was investigated, typically using one or more coupler forms per study [4, 6, 10–13], and the effect of some couplers on seismic column performance was investigated [14]. Bompaa and Elghazouli [5, 15] collected more than 350 test data points from the literature and carried out a statistical analysis of the coupler performance database. They find that the strain power of the splice (the coupler and its anchor bars) can be reduced from 19 percent to 92 percent by different couplers. They also find that the geometry of the coupler plays an important role in the efficiency of splicing. They did not, however, recommend any coupling model or define the coupling characteristics that could be used in ductile members. Overall, it can be concluded that the stress-strain behavior of the mechanically spliced bars differs from that of the integrated bars on the basis of the previous coupler test results in such a way that the deformation capacity of the mechanically spliced bars is smaller than that of the integrated bars. In other words, the integrated bars stretch more than the mechanically spliced bars of the same length [4]. In a threaded coupler, the bar ends

are threaded and connected by a long nut [5, 16]. The failure of threads, which prevents ultimate tensile strength, is one of the weaknesses in the bar connections Figure 1 a [4]. To achieve the highest tensile strength, a failure outside the coupler connection must occur. Few numerical studies have been performed on bar threaded couplers Figure 1 b [17]. In this research, by identifying the target area for bar failure, the potential area for failure could be modified, which could be very useful in assessing the position of the RC plastic hinge. On this basis, it is suggested that the latest research on bar threaded couplers be combined to introduce a few new couplers and their experimental reaction to the latter based on their behavior's numerical modeling. The designed model is used to assess the specimens' optimal configuration parameters later on. To achieve this goal, the numerical study included changes in the height and thickness of the mechanical couplers and bars, and the FEM failure mode also included bar or thread disconnection. Coupler specimens are categorized into different groups and simulated using the finite element method software. Two calibration simulations and four cases were designed and theoretically studied on the basis of the results of the numerical model. The specimens with these configurations shall be examined under a uniaxial tensile test for the identification of the most appropriate coupler schemes for splicing reinforcement bars.



(a) (b)
Figure 1. Types of failure in Threaded couplers [4]

In this study, two types of bars are evaluated: 1) Integrated bar and 2) Threaded coupler. The dimensions of the specimens and the bars and the configuration of the coupler are shown in **Figure 2**. The integrated bar is 32 mm in diameter and 760 mm in height (**Figure 2a**). The bar for threaded couplers has a diameter of 32 mm a height of 380 mm, for each bar **Figure 2 b**, and the coupler has an external diameter of 48 mm and an internal diameter of 32 mm with a length of 84 mm **Figure 2 c**. The steel reinforcement bars used for the experimental specimens were of type AIII. The properties of the bars were 0.3, 500 MPa, and 210 GPa for Poisson ratio, tensile strength, and elasticity modulus, respectively. The threaded coupler was used for splicing between bars. The coupler properties for Poisson's ratio, tensile strength, and elasticity modulus were 0.3, 600 MPa, and 210 GPa, respectively.

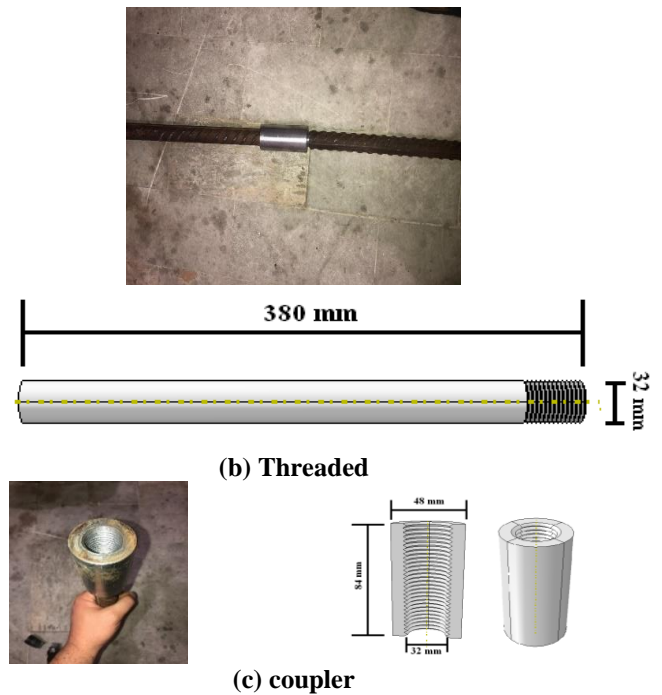
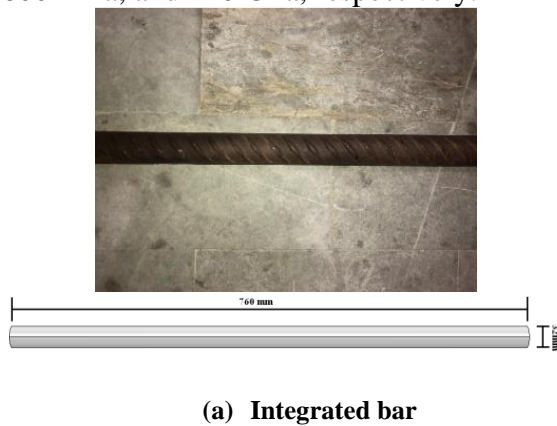


Figure 2. Experimental details and dimensions

2.2. Experimental test setup

This testing machine is used to apply tensile and compressive forces to round and flat samples, either statically or dynamically **Figure 3**. A maximum of 600 kN is applicable in the static state, and a maximum of 500 kN is applied in the dynamic state. The device consists of two jaws, the upper jaw has a support structure, and the lower jaw acts as a stimulus. The distance between the two jaws can be changed by raising and lowering the upper jaw. In addition, the jaws can be moved up to 30 cm apart. The digital controller 9600 is the intermediary between the device and the computer. In addition to precisely controlling the function of the mandible in both the elongation control and the force control, this controller is capable of sampling and transmitting two elongation signals (Stroke) and a force (Load) from the output of the converters installed on the actuator and the computer. It also provides two analog output channels for connecting to an external oscilloscope and viewing instantaneous elongation and load values. The entire set is controlled by the Workshop software package. This software package includes a number of programs. The

specimens of the integrated bar and the mechanical bar coupler were placed under uniaxial Tensile at the end of the bar. Specimens were tested under additive axial elongation of up to 20 mm (according to ASTM E8 [18]). The test setup is shown in **Figure 3**. The parts of the bar were first marked before starting the machine. The distance between the marks should be 6 times the diameter of the piece, and if the diameter of the bar is 32 mm, the range of the two targets should be 192 mm (according to ASTM E8 [18]). After the machine was turned on and checked, the air pressure was adjusted to 6 to 8 bars. Then the bar was firmly attached to the device, and the test was carried out. After testing, seeing the diagram, and breaking the rebar, its tensile strength was seen.

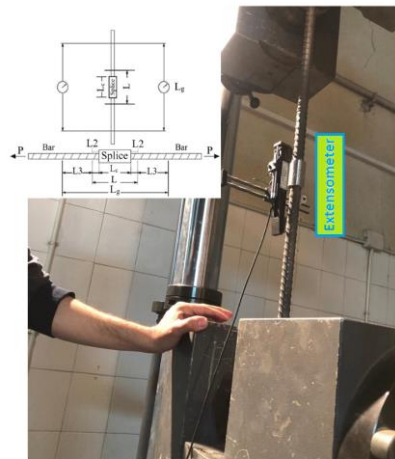


Figure 3. Testing configuration for uniaxial tests.

2.3 Results of bending tests

The results of the experimental bars integrated without coupler and with threaded coupler in terms of load, deflection, and relative yield elongation (d_y), maximum relative elongation (d_u), values of the general ductility ratio (μ) of the bar, dissipated energy, maximum capacity deformation, and failure modes are reported

in **Table 1**. The load- elongation curve response for both experimental cases is shown in **Figure 4**. These are divided into two main parts; the first part corresponded to a linear-elastic response with a constant slope that ended with the development of the first elongation, and the second part showed a nonlinear slope in both specimens, including the post elongation stage. **Figures 5-a** and **5-b** depict the failure modes of the experimented bars integrated without coupler and with threaded coupler respectively. Failure, observed for bar combined without coupling, near to Fixed Support and for threaded coupler, in the nearby coupling center. It should be noted that, on the basis of the mechanical splice requirements set out in ACI 318, section 12.14.3.4, "a full mechanical connection shall develop at least 125 percent of the specified bar strength when required by tension or compression [17]. This requirement means that, in the event of failure, the yield will occur in the reinforcement bar before the failure of the mechanical connection. As shown in **Figure. 5b**, a bar failure occurred in the coupler. Therefore, the splice used in this study does not meet this requirement.

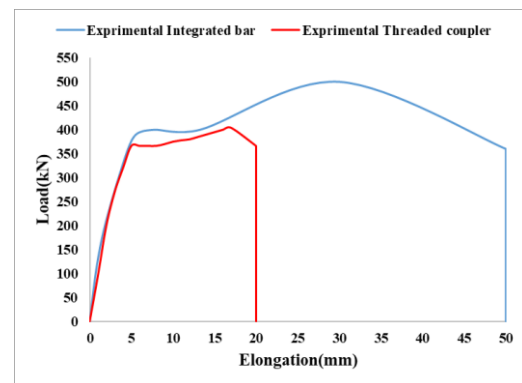


Figure 4. Load- elongation curves obtained by experimental results

Table 1. Experimental results

Specimen	Maximum Tensile strength (kN)	Fy	Deformation at the maximum capacity (mm)	d_y (mm)	d_u (mm)	dissipated energy (kN.mm)	$\mu = \frac{d_u}{d_y}$	Failure mode
integrated bar	500	400	30	8	50	25131	6.25	bar

Threaded coupler	404	366	17	5	17	6782	3.4	Thread
------------------	-----	-----	----	---	----	------	-----	--------

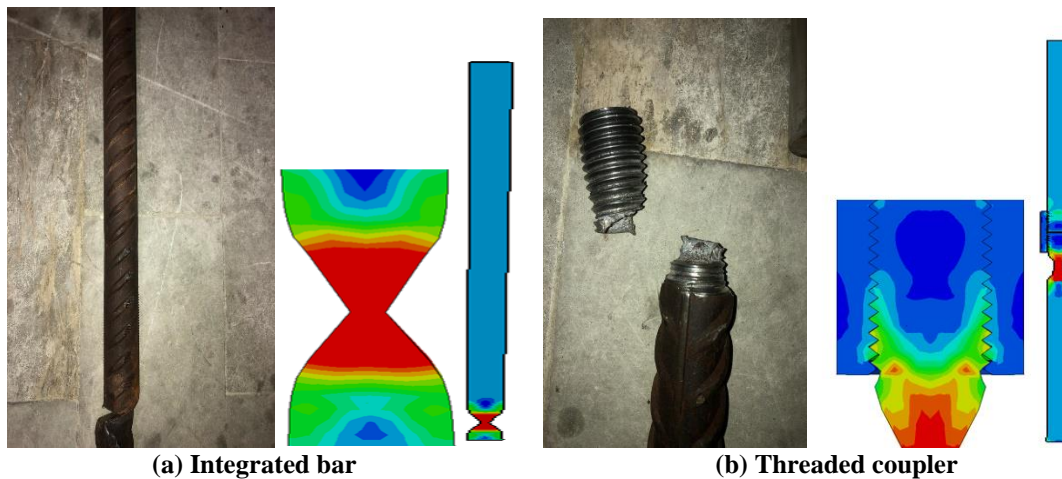


Figure 5. Failure mode

3. Finite element method (FEM)

ABAQUS[19] general purpose Finite element software was used to model experimental tests in order to provide a general procedure widely available for engineering. The following subsections deal with geometry, materials, mesh, boundary conditions, contacts, and calculation procedure definitions for the implemented model. The models were divided into three 3D parts: one for the integrated bar, one for the coupler, and the last one for the threaded bar. Models A to D are the numerical models that were designed by simulator software, and their corresponding dimensions are presented in **Figure 7**. In all experimental and numerical models, the dimension of the mesh is equal to the top surface of the threads. The interaction between the coupler and the thread was considered surface-to-surface contact. In order to simplify the computation, the trilinear model with isotropic hardening is adopted for the rebar and coupler. The model assumes a linear stress–strain relationship for the material prior to the yield stress. The hardening phase is simplified as a straight line after the yield plateau. For the simulation of the bar and coupler, two linear 3D truss elements (T3D2) were used. Various mesh sizes according to each part's thickness (bar and

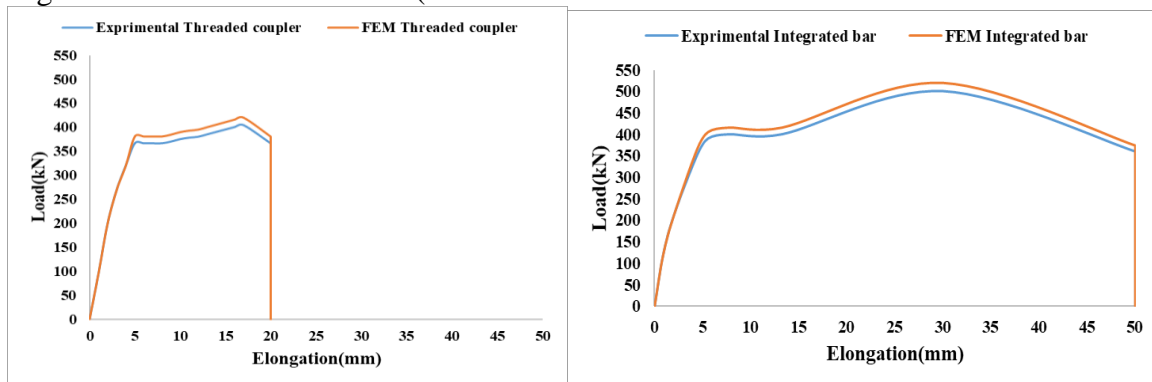
coupler) were applied. The convergence of digital solutions was controlled with mesh measurements of 100, 75, 50, and 25 mm in the concrete region.

3.1. Materials in FEM

Two experimental tests of the integrated bar and the threaded bar were chosen to fit the numerical model in the two main representative situations. The following parameters are used for the numerical simulation of the coupler, the integrated bar and the threaded bar: the nonlinearity of the geometric and material components of the elementary joints, the pretension force of the threaded rebar, the contact between the threaded thread, and the friction. The 6-node linear triangular prism element (C3D6) was used to model the coupler, the integrated bar and the threaded bar. The numerical results are highly sensitive to the properties of contact between the coupler components and the preloaded threaded bar. For all contacts, a small sliding surface-to-surface discretization method was considered. The surface contact properties between the plate elements were modeled as tangential behavior using a penalty friction coefficient of 0.40 Normal behavioral contact properties using Augmented Lagrangian Formulation were considered to be normal forces between the same components. Tangential contact between the coupler and the threaded bar

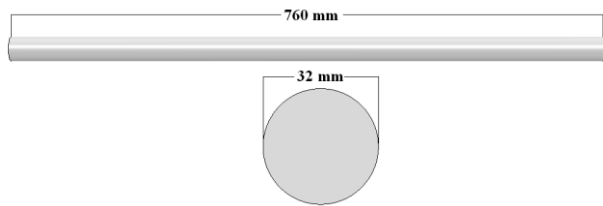
was considered to be frictional. The hard contact was used to link the coupler to the threaded bar elements[20]. Each coupler and the bar were considered to be a single body. The finite element predictions showed excellent agreement with the test results, in particular the lateral load-elongation response, reinforcement yield, crack patterns, and failure modes. The typical mechanical coupler bar is shown in **Figure 2**. In this study, the mechanical couplers bar was analyzed by the developed specimen and the results were compared with the experimental results **Figure 6**. As might have been considered in **Figure 6**, the results of the analytical samples are appropriately consistent with the results of the experimental studies. In particular, maximum loads were predicted with an average relative error of 4% (520 kN

predicted vs. 500 kN experimental for the cases with integrated bars and 420 kN vs. 404 kN for the cases with threaded coupler bars). A numerical model tends to consider a little more experimental load elongation capacity. A numerical model tends to be considered a little more experimental in terms of load elongation capacity. As long as the coupler-threaded bar contact was supposed to be completely bonded, when this condition is lost, model convergence is no longer possible, and there is no predicted data for the post-crisis response. Nevertheless, the FEM failure mode of FEM coupler-threaded disconnection and loading branch is the most significant for designing procedures, which was the initial aim of the research.

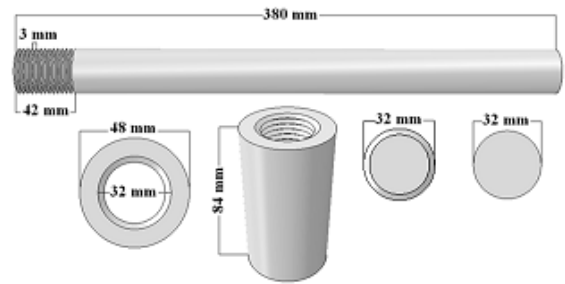


4. Geometric parameters study

To evaluate the performance of the coupler-threaded bar, various geometries were simulated with the parameters fixed in the previous fitting process. Simulated cases are summarized in **Figure 7**. The first step in evaluating a pair of threaded coupler bars is to guide the failure of the bars outside the thread. The threaded coupler bar cases were elongated at the ends of the bars. Cases were tested under additive axial elongation up to 50 mm. The coupler used had an elasticity modulus equal to 210 GPa, the Poisson ratio was 0.3, and the ultimate tensile strength was 600 MPa. Also, the steel used had an elasticity modulus equal to 210 GPa, the Poisson ratio was 0.3, and the ultimate tensile strength was 500 MPa.

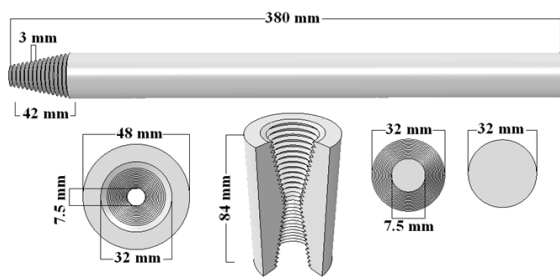


(1) Case integrate bar
Bar: 32 mm in diameter and 760 mm in height.



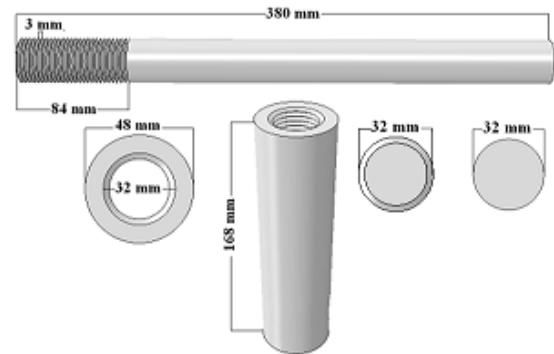
(2) Case threaded coupler

Bar: 32 mm in diameter and 380 mm in height.
Threads: 42 mm in height and 32 mm in external diameter.
coupler: 84 mm in height, 48 mm in external diameter, and 32 mm in inner diameter.



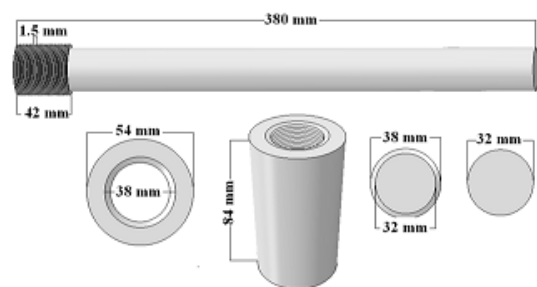
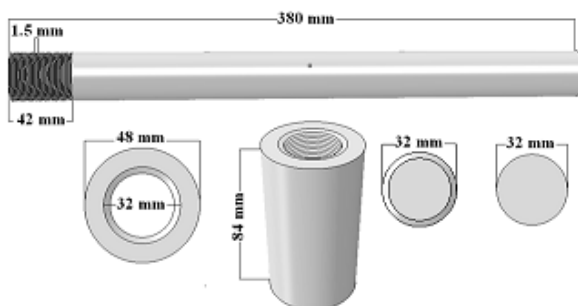
(3) Case A taper threaded coupler

Bar: 32 mm in diameter and 380 mm in height.
Threaded: 42 mm height, 7.5 mm high diameter, and 32 mm low diameter.
Coupler: 84 mm in height, 48 mm in external diameter, 32 mm in high diameter, and 7.5 mm in center diameter.



(4) Case B tall threaded coupler

Bar: 32 mm diameter and 380 mm height.
Threaded: 84 mm in height and 32 mm in external diameter.
Coupler: 168 mm height 48 mm external diameter and 32 mm inner diameter.



(5) Case C threaded with the teeth close together
 Bar: 32 mm in diameter and 380 mm in height.
 Threaded: 42 mm height, 32 mm external diameter, and the distance of each tooth is 1.5 mm.
 Coupler: 84 mm in height, the distance between each tooth is 1.5 mm, 48 mm in external diameter, and 32 mm in inner diameter.

(6) Case D oversize-threaded coupler
 Bar: 32 mm in diameter and 380 mm in height.
 Threaded: 42 mm height, 38 mm external diameter.
 Coupler: 84 mm in height, the distance between each tooth is 1.5 mm, 54 mm in external diameter, and 38 mm in inner diameter.

Figure 7. Definition of coupler, threaded bar and integrated bar specimens for geometry parametric study.

4.1 Analysis of the Load-Elongation Curves

The load-elongation curves of cases A, B, C, and D are shown in **Figure 8** together with those representing the experimental cases tested. In **Table 2**, the values of ultimate strength (F_p), maximum capacity deformation (F_u) and the area under the force-displacement curve (dissipated energy-Gd) are introduced. The results showed that the increased threaded bar cross section significantly increased the load-bearing capacity. Cases threaded coupler and B showed similar capacities, so increasing the height of the coupler is not really effective if the threaded bar-coupler connection is secured. Case B had a larger threaded area and therefore showed a higher initial stiffness, although the larger threaded area of Case C had a higher maximum resistance. In case C, the reduction of the distance between the teeth and the increased threaded amount in the center of the coupling cause the system to dissipate more energy compared to the threaded coupler case, although the maximum load-bearing capacity has not been maintained. In case C, with the reduction of threaded diameter in the form of a taper, the dissipated energy of the system was reduced, and the maximum load-bearing capacity was not maintained compared to the threaded coupler case. Comparing case D to case B, it has been shown that increasing the threaded section width is more effective than increasing the

threaded section height against elongation, as expected. Cases that integrated Bar and D showed similar capacities, making it very effective to increase the width of the threaded section.

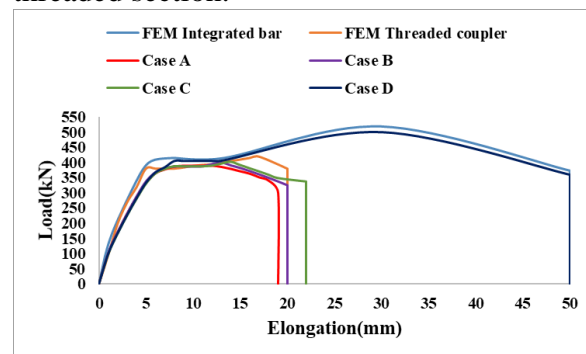


Figure 8. Comparison of Load-Elongation curves for cases.

4.2 Analysis of the Von Mises stress index

Until yielding, the material reaction may be believed to be nonlinear elastic, viscoelastic, or linear elastic. In material science and engineering, the Von Mises efficiency criteria could be formulated in terms of stress or comparable tensile stress. This is a scalar stress value that could be determined from the Cauchy stress tensor. In this case, the material was sidelined to start yielding when the Von Mises stress exceeded a value known as yield power. Note that Von Mises stress is a non-negative, scalar stress scale. Von Mises stress was widely used to present findings, and the structural safety of certain engineering components showed elastoplastic properties (e.g. steel or aluminum alloys) could be measured using

Von Mises stress. The maximum stress loss criterion of Von Mises was based on the theory of von Mises-Hencky, also known as the theory of scalar energy or the theory of maximum energy distortion. The principle notes that the ductile substance tends to yield at a position where the stress of Von Mises is equal to the stress limit. In most situations, the yield strength has been used as the tension maximum. The stress of Von Mises 5-007v could be represented by six stress components[21]. The model for the experimental case threaded coupler had maximum Von Mises stress value of about

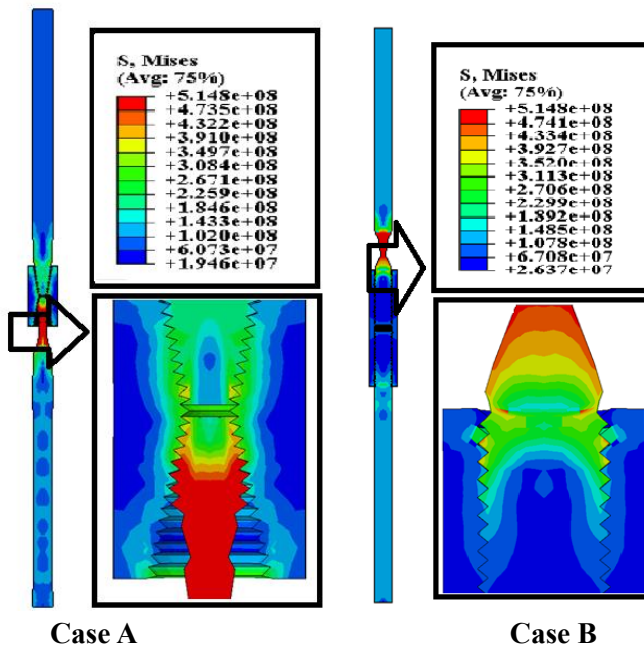
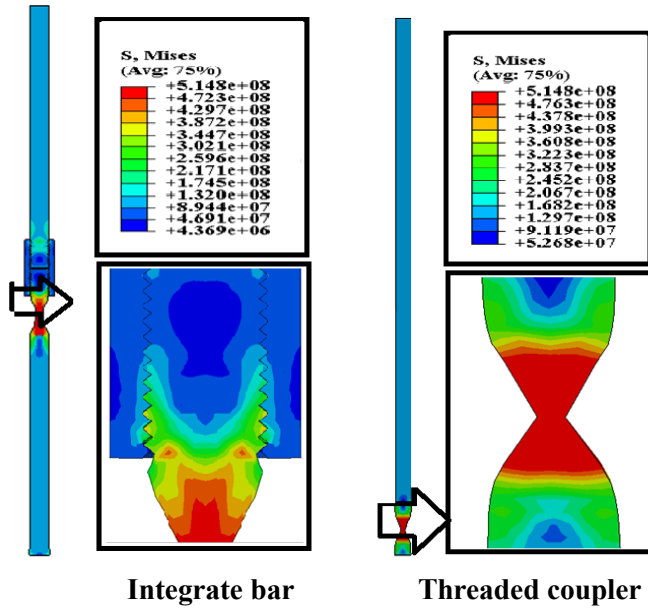
514 Mpa which indicated extensive tensile damage in the threaded coupler and most of the cracks were formed at the center of the coupler. The greatest cracks in this area were expected and obtained by the model, as can be seen in **Figure 9** and **Table 2**. If you put the coupler in, the maximum principal Von Mises stress is increased to about 534 Mpa, indicating a stress concentration and the corresponding damage increase.

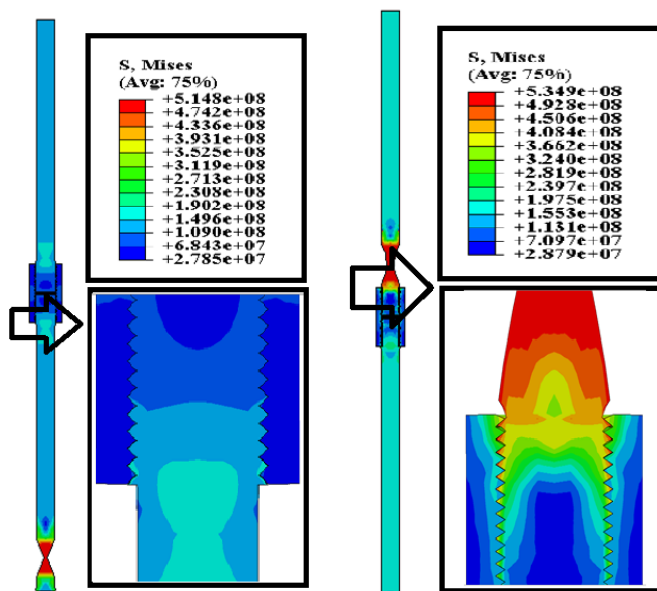
Table 2. The maximum load carrying capacity, the dissipated energy and maximum principle Von Mises stress for all the cases

Cases	Maximum Tensile strength (kN)	Deformation at the maximum capacity (mm)	dissipated energy (kN.mm)	Von Mises stress (Mpa)
FEM Integrated bar	520	30	21344	514
FEM Threaded coupler	420	17	7018	514
A	389.8	12	6155	514
B	400.5	13	6594	514
C	402	14	7297	534
D	500	30	20394	514

Due to unilateral stretching (similar to the FEM integrated bar), near-support failure was expected. Failure occurred at the thread location in specimens A, B, and C. The failure specimen D is similar to the base specimen near the support. The most damage at the thread site is related to the A specimen. This may be due to the low cross-section area. The results of specimen C show that lowering the thread pitch does not affect the fracture area, and the results of specimen C show that increasing the thread length does not affect the fracture area. Increasing the tooth height (case D) can significantly

improve the tensile capacity of the system and transfer the fracture out of the threaded region. In this case, Von Mises stress reached the greatest value among models: 20394 Mpa. This fact indicates that this case was the one that allowed more tensile damage develop in the bar. The case with the increased threaded height and coupler (case B) showed that threaded tensile damage had occurred. A representative contour plot of the Von Mises stress index is provided in Figure 8.





Case C

Case D

Figure 9. Maximum Von Mises stress in base and the proposed cases

potential equivalent to the integrated bar in all areas (1,2, and 3).

4.3 Dissipated energy

Energy dissipation and inelastic deformation of the elongation load resistance system suggest the ability of the structure to withstand the loading requirements of the seismic case. The sum of dissipated energy could be determined from the enclosed area at each loading stage, as shown by the monotonous response of the lateral load vs. the lateral elongation. The incorporation of dissipated energy related to the increase in lateral elongation will result in total dissipated energy at each stage of inter-story elongation. The evaluation of the dissipated energy for all case states is given in **Figure 10**. Dissipated energy is explored in three areas: areas 1, 2, and 3, with area 1 at a distance of 0 to 7 cm, area 2 at a distance of 7 to 14 cm, and area 3 at a distance of 14 to 20 cm. All cases were compared with the experimental case. The energy dissipation potential of cases A, B, and C was lower than that of the one integrated bar case in the corresponding case in After 3 loading steps. Case D has given an energy dissipation

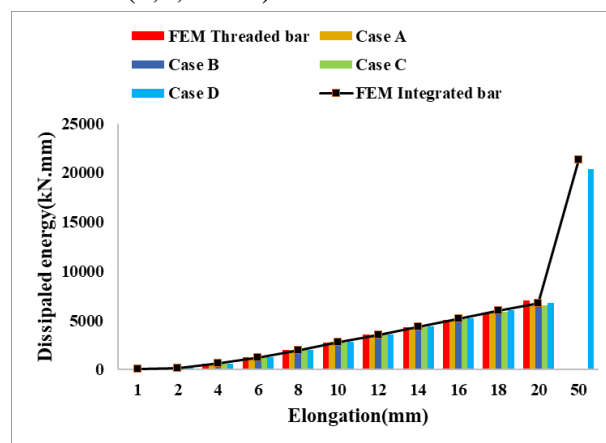


Fig. 10. Evaluation of the dissipated energy

4.4 Secant stiffness

The rigidity of a mechanical rebar coupler assembly could deteriorate as a consequence of reversal and repetitive monotonic loading behavior **Figure 11**[22]. During the elongation evaluation, the secant stiffness was estimated to determine the stiffness degradation, and the relationship was shown in **Figure 12** for all cases. The secant stiffness is taken as a straight-line slope connecting the peak loads at each step of the elongation at the positive displacements of the load versus the displacement envelope. Secant stiffness was investigated in three

zones, 1, 2, and 3, with zone 1 at a distance between 0 and 10cm, zone 2 at a distance between 10 and 20 cm, and zone 3 at a distance between 20 and 50 cm. The base case has been compared to all other cases. Cases A, B, and C have the same rigidity as integrated bar and threaded bar cases in areas 1 and 2, and the rigidity of zone 3 is lower than that of integrate bar and threaded bar cases. The stiffness of case D is the same as that of the integrated bar case in areas 2 and 3, and the stiffness of area 1 is more than that of the integrated bar case.

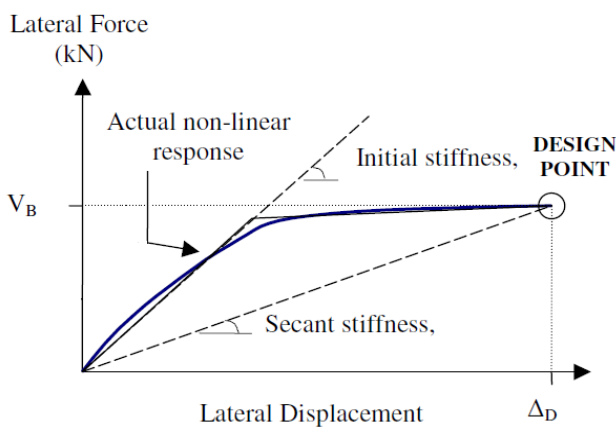


Figure 11. Usage of initial-stiffness and secant stiffness concepts related to the complete non-linear response of the structure and its equation[22]

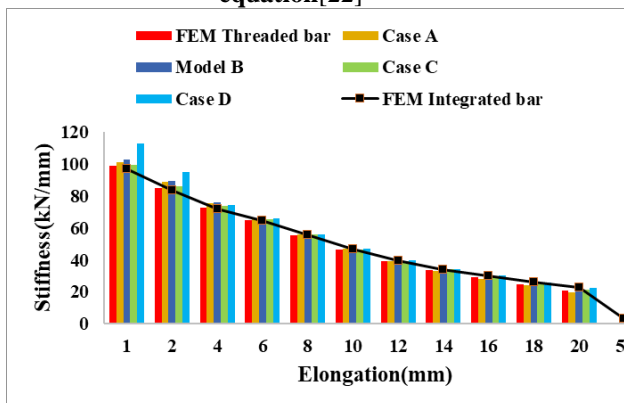


Fig.12. Evaluation of secant stiffness

5. Conclusions

In this study, a comprehensive experimental and analytical study was conducted to

investigate the performance of the threaded bar failure area. Based on the results of the numerical cases, different behavioral and performance indices such as tensile strength, ductility ratio, secant stiffness, and Von Misses are studied. The following results could be expressed in light of the stated subjects and within the limited scope of this study:

- ◆ Case D (oversize-threaded coupler) shows that the failure occurred in the rebar and outside the thread near the support; also, the Load-Elongation D strain curve is very similar to the integrated bar case. These results show the desirable performance of case D.
- ◆ Due to unilateral stretching (identical to the case integrated bar), failure near the support was expected. In the cases A (taper threaded coupler), B (tall threaded coupler), C (threaded with teeth close together), and threaded coupler, failure occurred at the thread position. Failure of the D (oversize-threaded coupler) case is similar to the integrated bar case near the support. The most damage to the thread site was related to the C case. This can happen due to the low cross-section area. Case D results show that lowering the thread pitch does not affect the fracture area, and case C results show that increasing the thread length does not affect the fracture area.
- ◆ Cases A, B, and C and threaded couplers have provided a lower energy dissipation capacity than the Integrate bar case. Among the various threaded couplers, the D arrangement has the highest increase in strength and energy dissipation capacity of the cases studied. Case D in areas 1 and 2 has the same stiffness as the case integrate bar, the stiffness in area 3 is less than the case integrate

bar. The stiffness of cases A, B, and C is not increased compared to the case integrated bar.

6. Acknowledgements

The authors would like to thank the logistical support provided by the IIEES (International Institute of Earthquake Engineering and Seismology in Tehran, Iran). Support is also gratefully acknowledged from the Cuboid Construction Company (Dr. Bahrani), the Foul Yazd Company (Eng. Ehramiyan), and the Sahand Mechanical Splice Company (Eng. Habibnezhad). This work is based upon research funded by Iran National Science Foundation (INSF) under PROJECT No.4013168.

7. References

- [1] Bai ASH, Ingham JM. Seismic performance of mechanically coupled reinforcing bars. *Magazine of Concrete Research* 2009;61:529–37. <https://doi.org/10.1680/macr.2008.00098>.
- [2] Hulshizer AJ, Ucciferro JJ, Gray GE. Mechanical Reinforcement Couplings Meet Demands of Strength and Constructibility. *Concrete International* 1994;16:47–52.
- [3] ACI Committee 318. *Aci 318 - 19 Building Code Requirements for Structural Concrete and Commentary*. 2019.
- [4] Nateghi-Alahi F, Shokrzadeh MR. Behavior considerations for mechanical rebar couplers. Behavior considerations for mechanical rebar couplers, University of Tokyo: 2019, p. 30–41.
- [5] Dahal PK, Tazarv M. Mechanical bar splices for incorporation in plastic hinge regions of RC members. *Construction and Building Materials* 2020;258:120308. <https://doi.org/10.1016/j.conbuildmat.2020.120308>.
- [6] Bompa D V., Elghazouli AY. Monotonic and cyclic performance of threaded reinforcement splices. *Structures* 2018;16:358–72. <https://doi.org/10.1016/j.istruc.2018.11.009>.
- [7] Department of Transportation. *Method of Tests for Mechanical and Welded Reinforcing Reinforcing Steel Splices* 2013:1–5.
- [8] ISO/DIS 15835. *Steel for the Reinforcement of Concrete - Reinforcement Couplers for Mechanical Splices of Bars (Parts 1 to 3)*. International Organization for Standardization, Geneva, Switzerland; 2018. n.d.
- [9] ASTM A1034/A1034M-10a. *Standard Test Methods for Testing Mechanical Splices for Steel Reinforcing Bars*. West Conshohocken, PA; 2015. 5 pp. n.d.
- [10] Henin E, Morcoux G. Non-proprietary bar splice sleeve for precast concrete construction. *Engineering Structures* 2015;83:154–62. <https://doi.org/10.1016/j.engstruct.2014.10.045>.
- [11] Lin F, Wu X. Mechanical Performance and Stress–Strain Relationships for Grouted Splices Under Tensile and Cyclic Loadings. *International Journal of Concrete Structures and Materials* 2016;10:435–50. <https://doi.org/10.1007/s40069-016-0156-5>.
- [12] Yuan H, Zhenggen Z, Naito CJ, Weijian Y. Tensile behavior of half grouted sleeve connections: Experimental study and analytical modeling. *Construction and Building Materials* 2017;152:96–104. <https://doi.org/10.1016/j.conbuildmat.2017.06.154>.
- [13] Liu H, Han Q, Bai Y, Xu C, Du X. Connection performance of restrained deformed grouted sleeve splice. *Advances in Structural Engineering* 2018;21:488–99.

- <https://doi.org/10.1177/1369433217719987>.
- [14] Han W, Zhao Z, Qian J, Cui Y, Liu S. Seismic behavior of precast columns with large-spacing and high-strength longitudinal rebars spliced by epoxy mortar-filled threaded couplers. *Engineering Structures* 2018;176:349–60. <https://doi.org/10.1016/j.engstruct.2018.09.007>.
- [15] Bompa D V., Elghazouli AY. Inelastic cyclic behaviour of RC members incorporating threaded reinforcement couplers. *Engineering Structures* 2019;180:468–83. <https://doi.org/10.1016/j.engstruct.2018.11.053>.
- [16] Kheyroddin A, Mohammadkhah A, Dabiri H, Kaviani A. Experimental investigation of using mechanical splices on the cyclic performance of RC columns. *Structures* 2020;24:717–27. <https://doi.org/10.1016/j.istruc.2020.01.043>.
- [17] ACI 318-19 Building Code Requirements for Structural Concrete and Commentary. 318-19 Building Code Requirements for Structural Concrete and Commentary 2019. <https://doi.org/10.14359/51716937>.
- [18] ASTM E8 / E8M - 16ae1 Standard Test Methods for Tension Testing of Metallic Materials n.d. <https://www.astm.org/Standards/E8> (accessed October 19, 2020).
- [19] ABAQUS. Abaqus User's Manual version 2019. Dassault Systèmes Simulia Corp: Providence, RI, USA 2019.
- [20] Nguyen KH, Kim HC, Shin H, Yoo YH, Kim JB. Numerical investigation into the stress wave transmitting characteristics of threads in the split Hopkinson tensile bar test. *International Journal of Impact Engineering* 2017;109:253–63. <https://doi.org/10.1016/j.ijimpeng.2017.07.004>.
- [21] J. Charabarty. *Theory of Plasticity*. 2006.
- [22] Shokrzadeh MR, Nateghi-Alahi F. Evaluation of hybrid NSM-CFRP technical bars and FRP sheets for seismic rehabilitation of a concrete bridge pier. *Bridge Structures* 2022;18:75–88. <https://doi.org/10.3233/BRS-290180>.